ACS APPLIED MATERIALS & INTERFACES

www.acsami.org

Research Article

Inhalation Delivery of Interferon-λ-Loaded Pulmonary Surfactant Nanoparticles Induces Rapid Antiviral Immune Responses in the Lung

Chan Hee Gil,[¶] Chanhee Oh,[¶] Jeongsoo Lee,[¶] Mincheol Jang,[¶] Junhee Han, Sung-Dong Cho, Su-Hyung Park,* Ji-Ho Park,* and Hyun Jik Kim*

Cite This: *ACS Appl. Mater. Interfaces* 2024, 16, 11147−11158

Read Online

ACCESS | Metrics & More | Article Recommendations | Supporting Information

ABSTRACT: The interferon-λ (IFN-λ)-regulated innate immune responses in the airway expand our understanding toward antiviral strategies against influenza A virus (IAV). The application of IFN-λ as mucosal antiviral therapeutic is still challenging, and advanced research will be necessary to achieve more efficient delivery of recombinant IFN-λs to the damaged respiratory mucosa. In this study, we examine the capability of IFN-λ to stimulate the innate immune response, promoting the swift elimination of IAV in the lungs. Additionally, we develop IFN-λ-loaded nanoparticles incorporated into pulmonary surfactant for inhalation therapy aimed at treating lung infections caused by IAV. We found that inhaled delivery of IFNλ-PSNPs significantly restricted IAV replication in the lungs from 3 days after infection (dpi), and IAV-caused lung histopathologic findings were completely improved in response to IFNλ-PSNPs. More significant and rapid attenuation of viral RNA was observed in the lung of mice with inhaled delivery of IFNλ-PSNPs compared to mice with recombinant IFN-λs. Inhalation treatment of IFNλ-PSNPs to IAV-infected mice can result in the increase of monocyte frequency in concert with restoration of T and B cells composition. Furthermore, the transcriptional profiles of monocytes shifted toward heightened IFN responses following IFNλ-PSNP treatment. These results imply that IFN-λ could serve as a robust inducer of innate immunity in the lungs against IAV infection, and inhalation of IFN-λs encapsulated in PSNPs effectively resolves lung infections caused by IAV through rapid viral clearance. PSNPs facilitated improved delivery of IFN-λs to the lungs, triggering potent antiviral immune responses upon IAV infection onset.

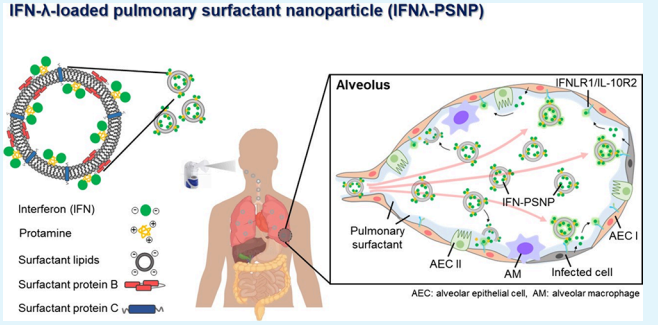

KEYWORDS: *influenza A virus, pulmonary surfactant, nanoparticle, interferon-λ, inhalation therapy*

INTRODUCTION

The innate immune system by producing interferon (IFN)s introduces substantial heterogeneity in host responses to viral infections, interacting with different viruses to influence antiviral defense mechanisms.[1,2] While IFN-λ exhibits certain functional overlaps with IFN-β, previous reports have elucidated a distinct role for IFN-λ in orchestrating immune defense against viral infections at mucosal and barrier surfaces.[3−5] IFN-λ possesses the ability to orchestrate defensive immunity against respiratory viral infections and is thought to be chiefly accountable for localized antiviral innate immunity against influenza A virus (IAV) in the respiratory epithelium, without inducing excessive tissue damage and inflammation.[6−9] Recently, the possibility that administration of IFNs ameliorates the virus-cause pathologic findings *in vivo* lung and strong restriction of SARS-CoV-2 replication by exogenous compensation of IFN-λ becomes apparent.[10] Our previous studies implicated that IFN-λs might be potent adjuvants capable of eliciting robust antiviral immunity and intranasal application of IFN-λs augments a defense mechanism against respiratory viral replication and virus-caused lung damage.[3,4,11] However, application of IFN-λ as mucosal antiviral therapeutic is still challenging, and advanced research will be necessary to achieve more efficient delivery of recombinant IFN-λs to the damaged respiratory mucosa, where respiratory virus directly invade.

The lung possesses large surface area lined with thin alveolar epithelium, pulmonary surfactant (PS), and high permeable and considerable vascularization, and these structural characteristics are closely related to the inhaled delivery of therapeutics to the lung.[12] In particular, PS is a mixture of

Received: September 13, 2023
Revised: February 3, 2024
Accepted: February 11, 2024
Published: February 26, 2024

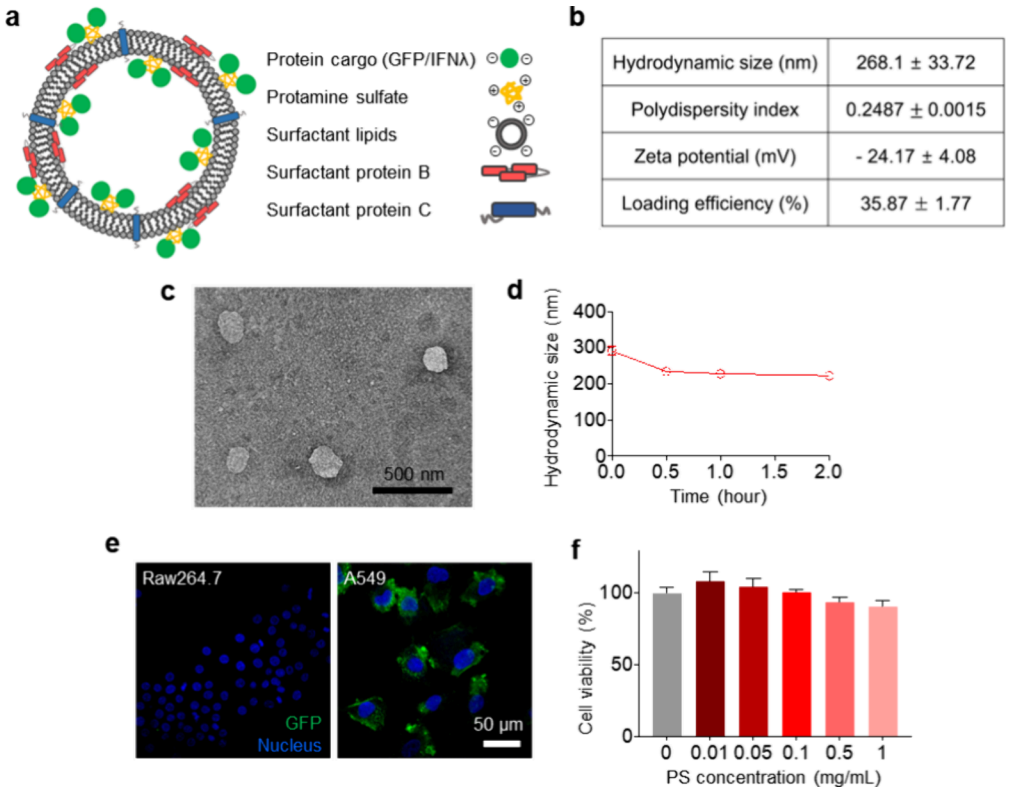

Figure 1. Preparation and characterization of GFP-loaded pulmonary surfactant nanoparticles (GFP-PSNPs). (a) Schematic illustration of GFP-PSNPs. (b) Hydrodynamic size, polydispersity index, surface charge, and GFP loading efficiency of GFP-PSNPs. (c) Transmission electron microscopy (TEM) image of GFP-PSNPs. (d) Colloidal stability of GFP-PSNPs in physiological condition. (e) Confocal fluorescence images of Raw264.7 and A549 cells after GFP-PSNP treatment: nucleus (blue, Hoechst), GFP (green). (f) Cytotoxicity of GFP-PSNPs after GFP-PSNP treatment at different concentrations. The data are presented as the mean ± SEM and analyzed by one-way ANOVA for (f).

lipids (~90%) and proteins (~10%) which is synthesized by type II alveolar cells and secreted into the alveolar space to reduce the surface tension in the alveoli air−liquid interspace, thus preventing alveolar collapse.[13] While the inhaled administration of therapeutics allows their efficient localization to the distal lung, the successful delivery of targeted materials often limited by a thin barrier composed of PS and optimal concentration of therapeutics is not effectively maintained at the level of alveolar epithelium.[14,15] Hydrophobic PS proteins B and C (PSP-B and PSP-C) incorporated in the vesicles are responsible for maintaining the mechanical integrity of PS layer in the dynamic environment by modulating the fusion and spreading of PS lipids.[16] Therefore, the transport of hydrophilic agents through the PS layer is more challenging for inhaled small molecules and proteins.[17]

In order to suppress the viral replication in the distal lung with IAV infection, IFN-λs must be delivered to the surface of infected epithelial cells in the lung without breaching the integrity of the PS layer. Here, we prepare an inhalable formulation of IFN-λs combined with natural PS to overcome the PS-derived biophysical barrier for efficient pulmonary delivery of IFN-λs throughout the alveolar region by active interactions with the endogenous PS barrier. We synthesize inhalable nanoparticles based on PS by interacting a protamine/IFN-λs nanocomplex with PS (IFNλ-PSNPs) via electrostatic interactions. Our results show that inhaled delivery of IFNλ-PSNPs mediates more potent host-protective immune responses in concert with the improvement of IAV-caused acute lung damage in the early stages of infection. In addition, our current research offers essential insights into the immune response dynamics triggered by IFNλ-PSNPs, along with the innate immune reactions regulated by IFN in the lungs of mice infected with IAV.

RESULTS/DISCUSSION

GFP-Loaded Nanoparticles Are Fabricated with PS Constituents. To optimize the formulation of PSNPs for inhaled delivery of IFN-λs to the distal lung of an *in vivo* mouse model, we first prepared for green fluorescent proteins (GFP)-loaded PSNPs (Figure 1a). GFP was used as a model cargo protein because it has a molecular weight and net negative charge comparable with those of IFN-$\lambda_{2/3}$ (Table S1). Since GFP (and IFN-λs) and PS were both negatively charged, protamine, a polycationic positively charged protein that is known as an antidote for heparin, was employed to engage both negatively charged molecules via electrostatic interactions. Various formulations of GFP-loaded PS particles were first prepared by hydrating the dried PS film with mixture solutions of GFP and protamine at different molar ratios. Among them, a formulation prepared at the GFP-protamine molar ratio of 1:10 was selected for subsequent experiments because it showed the highest loading efficiency with the appropriate hydrodynamic size and zeta potential (Figure S1A−C). The size of GFP-loaded PS particles was further controlled to the range of 100−400 nm for efficient inhalation delivery to the alveolar region by using an extrusion method. Hydrodynamic size, polydispersity index, and ζ potential of the resulting GFP−loaded PS nanoparticles (GFP-PSNPs) were 268 nm, 0.25, and −24 mV, respectively, and loading efficiency of GFPs in the PSNP was 35% (Figure 1b). TEM images

https://doi.org/10.1021/acsami.3c13677
ACS Appl. Mater. Interfaces 2024, 16, 11147−11158

revealed that GFP-PSNPs appeared spherical with an approximate physical size of 200 nm (Figure 1c) and that the colloidal stability of GFP-PSNPs was maintained in both nebulizing and physiological conditions (Figure 1d and Table S2).

We next examined whether PSNPs can mediate efficient delivery of the protein cargo to alveolar epithelial cells in an *in vitro* culture system. Raw264.7 murine macrophages and A549 human lung adenocarcinoma cells were chosen as models of alveolar macrophages and alveolar type II epithelial cells, respectively. The cells were treated with GFP-PSNPs and imaged using a confocal fluorescence microscope. Confocal fluorescence microscopy revealed that GFPs were highly localized in A549 cells, not in Raw264.7 macrophages (Figure 1e), indicating the preferential uptake in the alveolar type II epithelial cells that are responsible for the secretion and removal of PS. Such uptake of PSNPs did not induce significant cytotoxicity within the tested concentrations (Figure 1f). The GFP-protamine complexes without a PS coating were inefficient in delivering the protein cargo to both cells (Figure S2A,B). We then investigated whether PSNPs can mediate the efficient localization of the protein cargo in the lungs of C57BL/6 (B6) via inhalation delivery. In addition to the protein cargo, distribution and retention of surfactant lipids were tracked with DiR, lipophilic near-infrared (NIR) fluorescent dye, embedded in the surfactant lipid bilayer. DiR-labeled GFP-PSNPs or GFPs alone were inhaled to the nasal cavity of mice and immunofluorescence imaging of major organs was conducted. Fluorescence imaging of lungs revealed that significantly larger amount of GFP-PSNPs was distributed throughout the lung tissues while most of free GFPs was localized in the trachea (Figure 2a). Furthermore, the GFP-PSNP group showed higher GFP signal in the lungs over 72 h after inhalation delivery compared to the free GFP group. In other major organs such as liver, spleen, heart, and kidney, the GFP signal was barely detected (Figure S3, Figure 2b). As the inhalation dose increased, the pulmonary delivery efficiency increased only in the lungs (Figure 2c), ensuring that the lung was the only tissue specific for the GFP-PSNP signal.

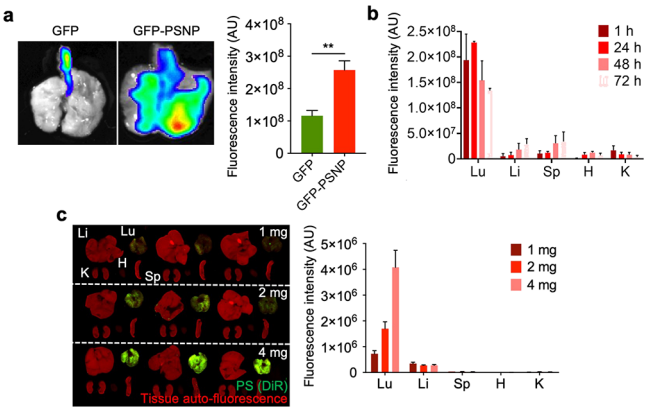

Figure 2. Biodistribution of GFP-PSNPs after inhalation delivery. (a) *Ex vivo* GFP fluorescence images of mouse lungs 1 h after inhalation of free GFPs and GFP-PSNPs. (b) Time-dependent biodistribution of GFPs after inhalation of GFP-PSNPs: lung (Lu), liver (Li), spleen (Sp), heart (H), kidney (K). (c) Dose-dependent biodistribution of GFPs after inhalation of GFP-PSNPs. The data are presented as mean ± SEM and analyzed by *t*-test for (a) and by two-way ANOVA for (b) and (c) (**$p < 0.01$; ns, not significant).

Collectively, these results suggest that the PSNP formulation can efficiently localize the protein cargo in an *in vivo* lung after inhaled delivery.

Inhaled Delivery of IFNλ-PSNPs to the Lungs. We next assessed whether PSNPs loaded with IFN-λs were distributed well in the lung tissue of mice after inhaled delivery. IFNλ-PSNPs were prepared based on the protocol for GFP-PSNPs. Hydrodynamic size, polydispersity index, and ζ potential of the resulted IFNλ-PSNPs were 242 nm, 0.18, and −29 mV, respectively, and loading efficiency of IFN-λs in the PSNP was 32% (Figure 3a). TEM coupled with immunogold labeling revealed that the IFN-λs were attached on the inside and surface of the PSNP (Figure 3b). IFNλ-PSNPs maintained the colloidal stability in the physiological condition (solution containing 10% serum at 37 °C) over the tested time period (Figure 3c). Next, we investigated whether PSNPs can mediate the efficient localization of IFN-λs in the alveolar region of the lungs following inhaled delivery. The lung tissues were harvested for immunofluorescence imaging 1 and 3 days after the inhalation of IFNλ-PSNPs or IFN-λs alone. The results revealed that a significant fluorescence intensity of IFN-λs was found along the alveolar surface when formulated in the PSNP (Figure 3d). Furthermore, the level of IFN-λs in the alveolar region increased until 3 days after the inhaled delivery of IFNλ-PSNPs (Figure 3e). These results indicate that PSNPs promote an efficient localization of IFN-λs in the alveolar region of *in vivo* lung and IFN-λs was delivered into the lung combined with PSNPs without breaching the integrity of endogenous PS layer. Our data showed that PSNP formulation enabled efficient and prolonged localization of IFN-λs along

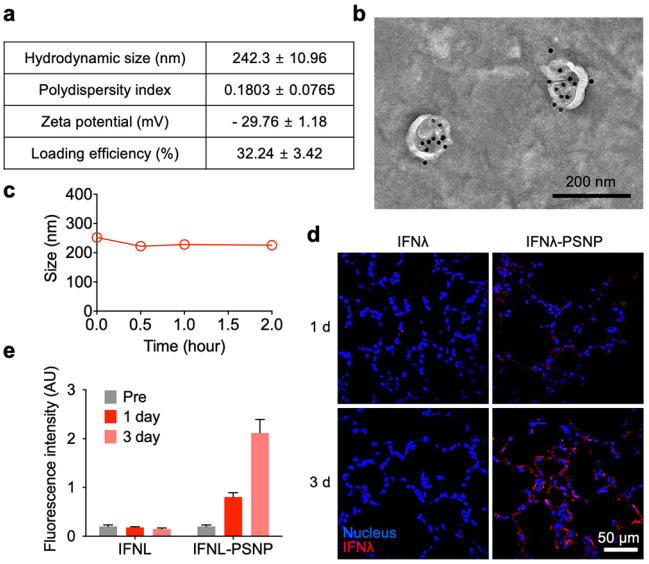

Figure 3. Physicochemical and biological characterization of IFNλ-loaded pulmonary surfactant nanoparticles (IFNλ-PSNPs). (a) Hydrodynamic size, polydispersity index, surface charge, and IFNλ loading efficiency of IFNλ-PSNPs. (b) TEM image of IFNλ-PSNPs. Black dots indicate gold nanoparticles attached to IFNλ molecules on the surface of PSNPs. (c) Colloidal stability of IFNλ-PSNPs in physiological condition. (d) Confocal fluorescence images of alveolar region of the lungs 1 day and 3 days after IFNλ-PSNP inhalation: nucleus (blue, Hoechst), IFNλ (red). (e) Quantitative fluorescence graph of (d). Pre indicates the fluorescence before inhalation. The results are presented as the mean ± SEM and analyzed by one-way ANOVA for (e).

https://doi.org/10.1021/acsami.3c13677
ACS Appl. Mater. Interfaces 2024, 16, 11147−11158

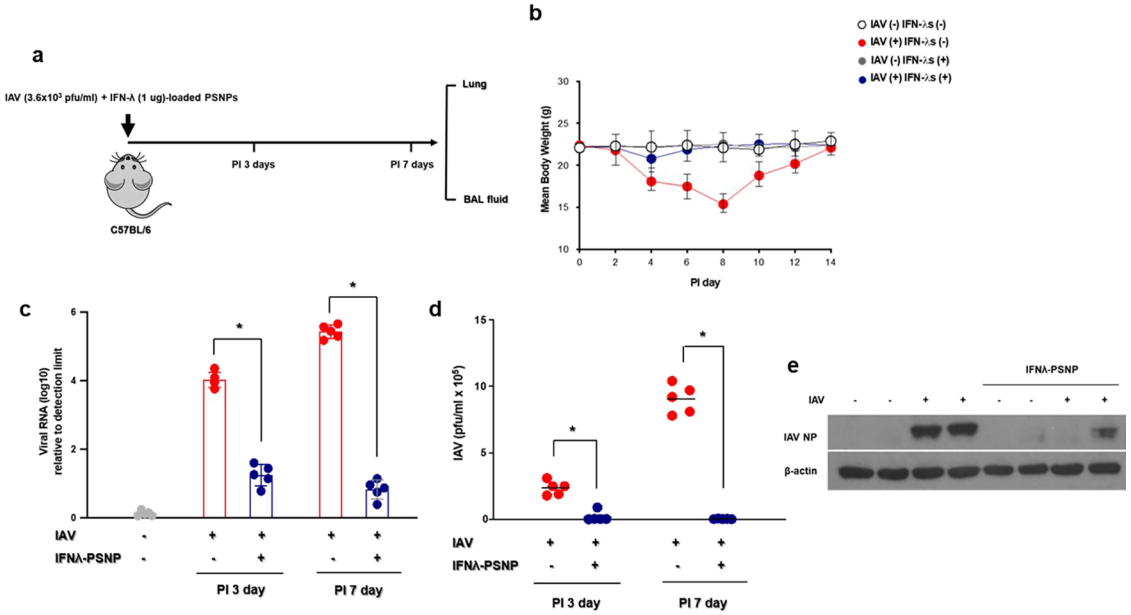

Figure 4. Inhaled delivery of IFNλ-PSNPs restricts IAV replication in an *in vivo* lung. (a) Schematic experimental design for IAV infection and inhaled delivery of IFNλ-PSNPs. C57BL/6 mice were administered with IFNλ-PSNPs (IFN-λ2, 1 μg; IFN-λ3, 1 μg) via inhaled delivery following IAV infection (3.6×10^3 pfu IAV WS/33 (H1N1, 3 dpi (N = 5), 7 dpi (N = 5)). (b) Changes in the mean body weights of the mice were compared according to IAV infection and inhaled delivery of IFN-λ. (c) IAV *PA* RNA levels in lung tissue, (d) viral titer in BAL fluid, and (e) IAV nucleoprotein were determined at 0, 3, and 7 dpi. The real-time PCR results were analyzed by the Mann−Whitney U test and are presented as mean ± SD values from three independent experiments. *$p < 0.05$ vs noninfected mice.

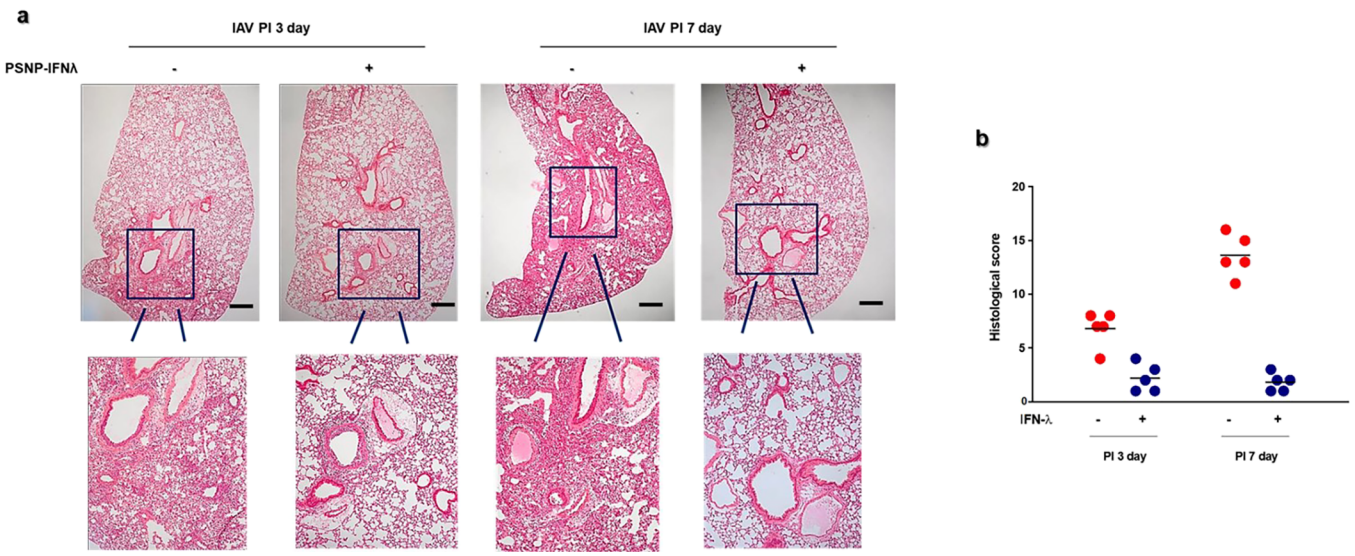

Figure 5. Inhaled delivery of IFNλ-PSNPs reduces IAV-caused lung damage in an *in vivo* lung. (a) H&E-stained micrographs were also generated from lung sections of mice obtained at indicated time point of IAV infection (scale bar, 100 μM). (b) Histologic score of lung sections from mice obtained at indicated time point of IAV infection. Micrographs shown are representative of lung sections from five mice and were used to assess inflammation and tissue damage and to calculate a histological score.

the alveolar region and subsequently promoted the production of ISGs from alveolar epithelial cells.

Inhaled Delivery of IFNλ-PSNPs Restricts IAV Replication in the Lungs. B6 mice were infected with IAV via intranasal inoculation (3.6×10^3 pfu/ml) (Figure S4A) and a significant decrease in mean body weight was observed in mice with IAV infection from 6 days post infection (dpi) until 12 dpi (Figure S4B). The mean level of IAV RNA, viral titer, and nucleoprotein level showed significant elevation from 3 dpi onward, with the highest titer at 7 dpi (RNA level, 3.96×10^4; viral titer, 6.1×10^5 pfu/mL) and gradually decreased until 14 dpi in the lung of IAV-infected mice (Figure S4C−E). Histological analysis of the lungs also revealed the extensive infiltration of inflammatory cells in IAV-infected mice at 7 dpi (Figure S4F).

As a next step, IFNλ-PSNPs were administered to B6 mice (N = 5) following IAV infection through inhaled delivery to determine the antiviral therapeutic effect of IFN-λs (Figure 4a). B6 mice treated with IFNλ-PSNPs via inhalation did not show noticeable weight loss until 7 days dpi. Their average body weight remained above 20 g until 7 dpi, leading to a 100% survival rate among mice following IAV infection (Figure

https://doi.org/10.1021/acsami.3c13677
ACS Appl. Mater. Interfaces 2024, 16, 11147−11158

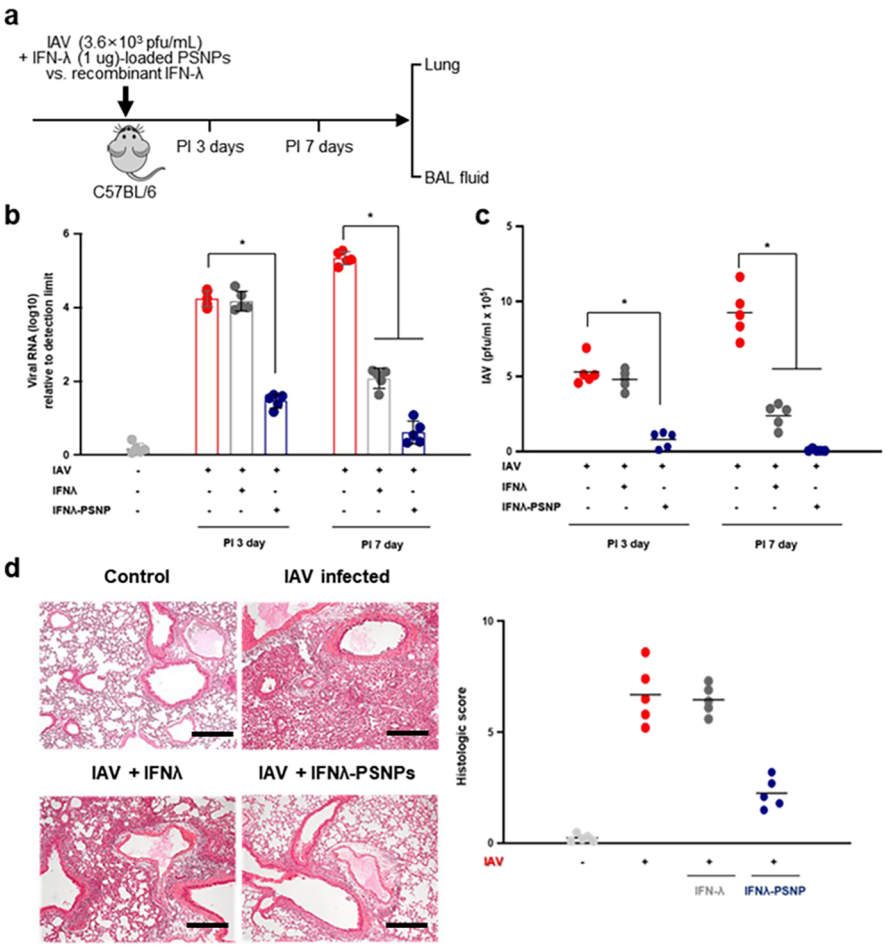

Figure 6. IFNλ-PSNPs induced more effective antiviral immune responses in the lung of IAV-infected mice. (a) Schematic experimental design for IAV infection and inhaled delivery of recombinant IFN-λs and IFNλ-PSNPs. C57BL/6 mice were administered with IFNλ-PSNPs (IFN-λ_2, 1 μg; IFN-λ_3, 1 μg) and same concentration of recombinant IFN-λs via inhaled delivery following IAV infection (3.6×10^3 pfu IAV WS/33 (H1N1, 3 dpi ($N = 5$), 7 dpi ($N = 5$)). (b) IAV *PA* RNA levels in lung tissue and (c) viral titer in BAL fluid were determined at 0, 3, and 7 dpi. (d) H&E-stained micrographs were also generated from lung sections of mice obtained at indicated time point of IAV infection (scale bar, 100 μM). The micrographs displayed represent lung sections from five mice, serving to evaluate inflammation and tissue damage and to determine a histological score. Real-time PCR findings were scrutinized using the Mann−Whitney *U* test and are depicted as mean ± SD values derived from three distinct experiments. *$p < 0.05$ vs noninfected mice.

4b). Compared to mice infected with IAV (4.01×10^4), those with IFNλ-PSNPs following IAV infection showed lower lung IAV *PA* RNA levels (0.87×10^2) at 3 dpi (Figure 4c). Inhaled delivery of IFNλ-PSNPs also reduced viral titer in the BAL fluid from mice infected with IAV (Figure 4d) and attenuated the IAV NP level significantly in the lung tissue (Figure 4e). In addition, the abnormal histologic findings in the lung of IAV-infected mice were completely reduced in response to inhalation delivery of IFNλ-PSNPs from 3 days postinfection (dpi) (Figure 5a,b). These findings demonstrated that inhaled delivery of IFNλ-PSNPs impeded IAV replication in the lung and improved acute viral lung infection through the rapid induction of antiviral responses. Inhaled delivery of IFNλ-PSNPs reduced viral replication significantly in the lung of IAV-infected mice from 3 days after infection. In addition, histopathologic findings of lung were completely improved in IAV-infected mice in response to IFNλ-PSNPs at early stage of infection. In comparison with the mice with inhalation of IFN-λ itself, IFNλ-PSNPs exhibited more potent antiviral effect after onset of infection after inhalation and the effect would be prolonged until 7 days of infection in concert with minimal viral replication and improvement of lung pathologic findings. These results demonstrate that the PSNP formulation can maximize therapeutic effects of inhaled IFN-λs by penetrating the PS layer and interacting with influenza virus in the lung tissue with evading alveolar macrophage uptake. Interestingly, both PS and protamine used in our therapeutic model were currently described in humans and it is expected to provide evidence for the development of inhaled therapeutic agents to suppress the respiratory virus in human lung. Since IFN-λ-specific receptors are dominantly existed in epithelial cells, the delivery of IFN-λs was determined to significantly increase innate immune responses at the level of respiratory epithelium compared to other types of IFNs.[10,18]

Inhaled Delivery of IFNλ-PSNPs to the Lung Induced Rapid Innate Immune Responses during IAV Infection. The quick transfer of antiviral properties through the inhalation of IFNλ-PSNPs prompted us to determine whether more potent protection could be achieved by IFN-λs combined with PSNPs. To this end, B6 mice were administered with IFNλ-PSNPs through inhalation and compared the antiviral properties to IAV-infected mice with inhaled delivery of recombinant IFN-λs (free IFN-λs) on 0, 3, and 7 dpi (Figure 6a). The real-time PCR showed remarkably

https://doi.org/10.1021/acsami.3c13677
ACS Appl. Mater. Interfaces 2024, 16, 11147−11158

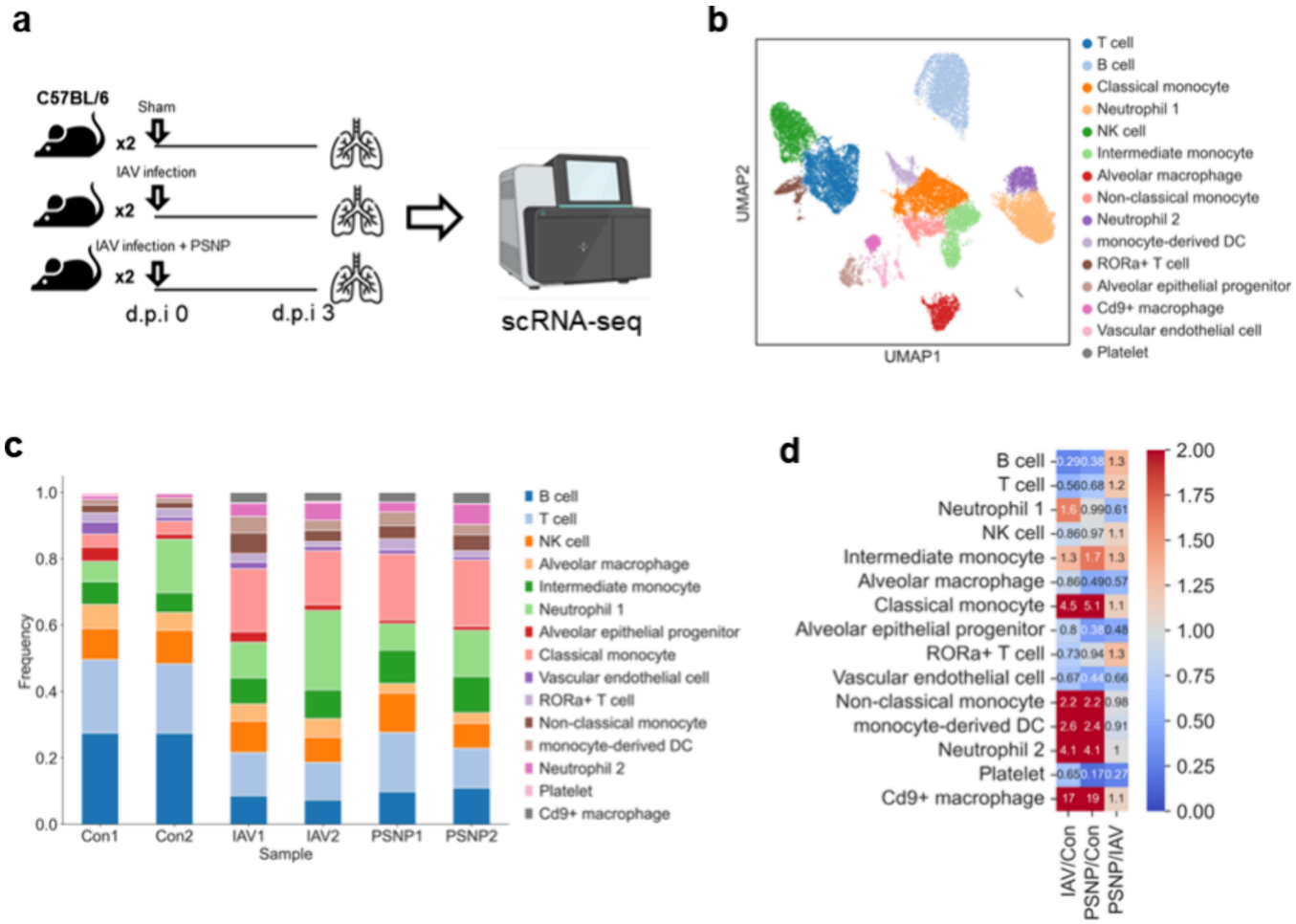

Figure 7. Single-cell RNA sequencing shows differential expansion of immune cells in IAV-infected mice. (a) Experimental scheme of scRNA-seq of the whole lungs of mice. (b) Unbiased UMAP clustering of the cells in the lungs. (c) Frequencies of clusters in each mice group. (d) Ratios of frequencies between mice groups for each cell cluster.

reduced viral RNA levels in IAV-infected mice in response to the inhaled delivery of IFNλ-PSNPs at 3 and 7 dpi. Inhaled delivery of same concentration of free IFN-λs also attenuated viral RNA level at 7 dpi but significant reduction of viral RNA was not observed in the lung of mice with free IFN-λs at 3 dpi (Figure 6b). The increased viral titer was also reduced in the BAL fluid of mice with inhalation of IFNλ-PSNPs following IAV infection at 3 and 7 dpi. While inhaled delivery of free IFN-λs could reduce the viral titer at 7 days postinfection (dpi), it did not decrease the viral titer at 3 days postinfection (Figure 6c). In addition, IAV-caused histopathologic findings of lung was clearly improved with inhaled delivery of IFNλ-PSNPs at 3 dpi, but free IFN-λs-inoculated mice still exhibited severe inflammation in the lung after IAV infection (Figure 6d). Interestingly, the real-time PCR results showed that mRNA levels of signature interferon-stimulated genes (ISGs) such as *Mx1*, *Ifitm1*, *Ifit2*, *Rsad2*, *Cxcl10*, and *Isg15* were significantly lower in the lung except *Ifitm1* with improvement of IAV-caused inflammation following inhaled delivery of IFNλ-PSNPs (Figure S5).

To assess the antiviral effect of inhaled delivery of IFN-βs, both free IFN-λs and IFNβ-PSNPs (1 ug IFN-β_1/mouse) were administered to B6 mice through inhaled delivery with following IAV infection. Compared to mice infected with IAV alone (4.2×10^4), IAV-infected mice did not exhibit the reduction of IAV RNA in response to inhalation of recombinant IFN-βs but those infected with IFNβ-PSNPs following IAV infection showed slightly lower IAV *PA* RNA levels (2.1×10^2) in the lung at 3 dpi. However, IAV RNA levels were not reduced in the lungs of IAV-infected mice with inhaled delivery of both recombinant IFN-βs and IFNβ-PSNPs at 7 days postinfection (dpi) (Figure S6A). The increased viral titer was not reduced in the BAL fluid from mice treated with inhalation of IFNβ following IAV infection at 3 and 7 dpi, even if IFNβ was delivered combined with PSNPs (Figure S6B). The extensive histologic findings in the lung of IAV-infected mice were not improved following inhaled delivery of IFNβ-PSNPs at 3 and 7 days postinfection (dpi) (Figure S6C). Based on these findings, we found that inhaled delivery of IFN-λs suppressed IAV infection in an *in vivo* lung, but the faster protection might be offered against IAV when IFN-λs were combined with PSNPs. The antiviral effect of IFN-β might be more limited compared to IFNλ-PSNPs in IAV-infected *in vivo* lung, even though it was delivered combined with PSNPs. Until now, research on inhaled IFN-β therapy has shown a notable antiviral impact in the lungs, leading to decreased asthma exacerbations. The dynamics of IFN-β underscore the possibility of using periodic prophylactic doses of exogeneous IFN-β to regulate viral infections in the respiratory system.[19] However, our data revealed that inhalation of IFNλ-PSNPs in the lungs of IAV-infected mice exhibited a more potent effect to improve acute IAV-caused lung damages and the potential

https://doi.org/10.1021/acsami.3c13677
ACS Appl. Mater. Interfaces 2024, 16, 11147−11158

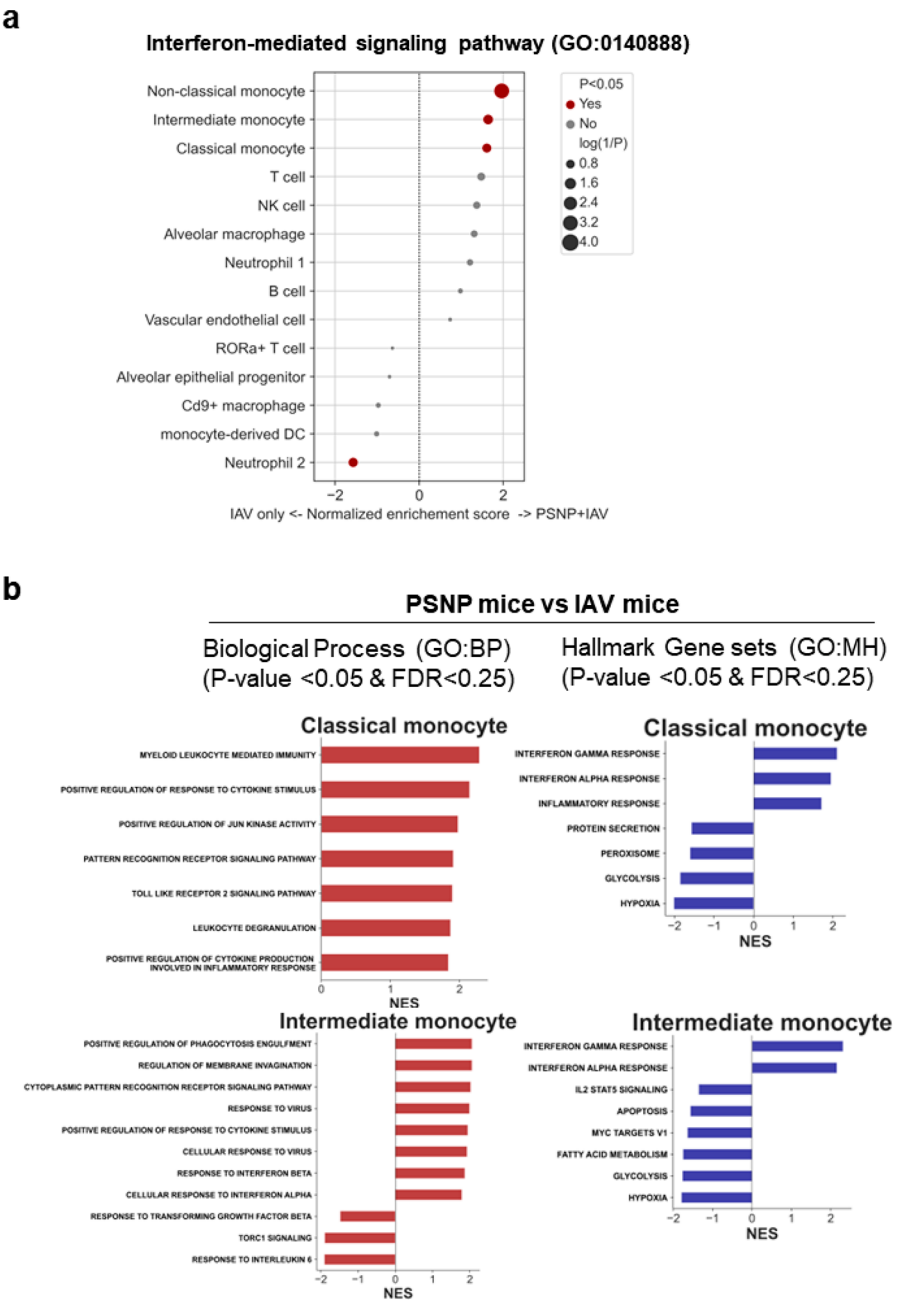

Figure 8. Single-cell RNA sequencing reveals the effects of PSNP on monocytes in IAV-infected mice. (a) GSEA using interferon-mediated signaling pathway gene set on each cell cluster of IAV only and PSNP mice show significant enrichment in monocytes of PSNP mice. (b) Classical and intermediate monocytes in PSNP are significantly enriched in interferon-response and effector functions-related gene sets.

of IFN-λ was sustained for a longer time than inhalation of IFN-β, even if IFN-β was delivered into the lung combined with PSNPs.

Single-Cell Transcriptomes of the Lung from IAV-Infected Mice Show Enhanced Interferon Responses after Inhaled Delivery of IFNλ-PSNPs. To investigate the detailed immunological changes by inhaled delivery of IFNλ-PSNPs in the lungs of IAV-infected mice, we performed scRNA-seq using the 10× Genomics platform. The whole lungs were harvested from the 3 groups of mice: uninfected control (N = 2), IAV infection only (N = 2), and IAV infection with inhaled IFNλ-PSNPs (N = 2) at two different time points, before the infection (0 and 3 dpi (Figure 7a). A total of 19 740 cells were acquired after quality-control. After batch correction with Harmony,[20,21] unsupervised clustering with uniform manifold approximation and projection (UMAP) distinguished 15 distinct clusters, which were annotated with corresponding cell types using representative marker genes (Figures 7b and S7). To analyze dynamic changes of immune response induced by IFNλ-PSNPs, we compared the relative frequency of immune cells among the control group and IAV infection with or without IFNλ-PSNPs groups. In contrast to control mice, the immune cell components were mainly comprised of neutrophils, monocytes and macrophages in the lungs of mice with IAV infection and with IAV plus inhaled delivery of IFNλ-PSNPs (Figure 7c). Both classical and other nonclassical monocytes were abundant in the lungs of IAV-infected mice, and this was more prominent in the lungs of mice with IAV

https://doi.org/10.1021/acsami.3c13677
ACS Appl. Mater. Interfaces 2024, 16, 11147−11158

infection plus IFNλ-PSNPs treatment (Figure 7d). The composition of T and B cells were decreased in the lungs of IAV-infected mice compared with control group, but they were increased in response to inhaled delivery of IFNλ-PSNPs compared with only IAV infection group (Figure 8a). To further characterize the increased subtypes of monocytes in the IAV infection plus IFNλ-PSNPs treatment group compared with the IAV infection-only group, the differentially expressed genes (DEGs) for monocytes were analyzed in terms of gene ontology (GO) biological process database and hallmark gene sets using gene set enrichment analysis (GSEA) (Figure 8b). Among the subtypes of monocytes, classical monocytes exhibited marked enrichment of genes related to cytokine stimulation and production involved in inflammatory response, pattern recognition receptor signaling pathway and leukocyte degranulation. Moreover, intermediate monocytes showed significant enrichment of genes related to viral clearance such as type I IFN response, cytokine stimulation, and phagocytosis engulfment (Figure 8b). Furthermore, both classical and intermediate monocytes exhibited prominent enrichment of genes involved in interferon responses such as "interferon-γ response" and "interferon-α response". Taken together, our results suggest that inhalation treatment of IFNλ-PSNPs to IAV-infected mice can result in the increase of monocyte frequency and enhanced IFN responses in concert with restoration of T and B cells composition.

Our findings suggest that prominently increased monocytes in response to IFNλ-PSNPs at 3 dpi may be effective in eliminating IAV and this is supported by the IFNλ-PSNP-stimulated restoration of T and B cell composition in the lung. Based on scRNA-seq data, we could infer that the proliferating monocyte cluster was dominant in the lung of IAV-infected mice, and the variability of monocyte composition was lessened in response to inhaled delivery of IFNλ-PSNPs. We found that IFNλ-PSNP-responsive monocytes exhibited DEGs enriched in GO terms mainly associated with "regulation of membrane invagination", "positive regulation of phagocytosis engulfment", "interferon-γ response", and "interferon-α response" at the early stage of infection. Inhaled delivery of IFNλ-PSNPs might alter the proportions of immune cells in concert with transcriptional changes in the lung of IAV-infected mice. Therefore, our current investigation offers crucial insights into the immune response patterns triggered by IFNλ-PSNPs, alongside the innate immune reactions in the lungs of mice infected with IAV, regulated by IFN. As like immune-modulatory treatments, inhalation therapy of IFN-λ is thought to provide a more effective therapeutic option for the treatment of lung infections caused by respiratory viruses, and this proposes important insights to aid the future design of the innate immune inducer acting locally on the respiratory tract.

CONCLUSION

In the present study, we found that inhaled delivery of IFN-λs induced potent antiviral immune responses in the lung and improved lung damage at an early stage of IAV infection when they were loaded with PSNPs. The present study implies that IFNλ-PSNPs are a potential therapeutic for controlling acute viral lung infection through the robust of innate immune responses in an *in vivo* lung and proves the usefulness of PSNPs as a vehicle of inhaled drug delivery to the alveolar lesion of lung. When a respiratory virus enters the host via the mucosal epithelium of oral and nasal cavities, it first initiates the protective mechanisms in the upper and lower respiratory tract.[22−24] The respiratory epithelium houses a distinct innate immune system designed to counteract invasion by respiratory viruses. Heightened innate immune reactions alleviate the disease burden in infected persons by strengthening antiviral defenses and enhancing tolerance to the illness.[25−31] The heightened secretion of IFN facilitates innate immune reactions, assisting in the elimination of viruses in the nasal or respiratory epithelium.[3,4,32] The established literature extensively discusses the functions of both IFN-α and -β in orchestrating the innate immune response and governing the subsequent adaptive immune activation.[33,34] In recent findings, it was discovered that IFN-λs can trigger antiviral immune reactions within the respiratory epithelium of live lungs, and augmenting IFN-λ levels can shield the host from the spread of respiratory viruses.[35−37] Previous studies from our research team indicate that IFN-λ may exert a more pronounced protective effect on the innate immune response during respiratory viral infections targeting the nasal epithelium. Additionally, administering IFN-λs intranasally proved to be more effective in controlling acute respiratory viral infections in animal models.[4,7] We hypothesized that the close relationship with IFN-λ could potentially aid the host respiratory tract in limiting influenza virus infection. Our findings indicated that administering IFN-λs through inhalation led to a near-complete reduction in viral titer in the lungs of mice infected with IAV, accompanied by a significant decrease in lung inflammation mediated by ISGs.

Alveolar type II epithelial cells secret high levels of ISGs in response to respiratory virus infection and subsequent secretion of IFNs,[38,39] and delivering the considerable amount of IFN-λs into the alveolar region can further enhance antiviral activity against IAV. The efficacy of inhaled IFN-λs depends upon their loco-regional distribution in the lungs, and an efficient mediator might be required to deliver IFN-λ through the PS barrier to the distal lung in human. Although various nanoparticle formulations have been developed for inhalation delivery, their efficient transport to the alveolar epithelium was impeded by alveolar macrophages and a thin and continuous PS layer,[40,41] thus reducing the therapeutic efficacy. Therefore, we developed a nanoparticle formulation composed of clinically used exogenous PS for efficient inhaled delivery of IFN-λs.

The fact that viral lung infection can be suppressed only with simultaneous administration seems to have limitations as a drug that can actually be applied to the human respiratory tract. However, the respiratory mucosa of humans and the lung tissue of mice are thought to have different characteristics, and since humans are fully equipped with other immune functions at the respiratory mucus, pulmonary surfactant, and nasal mucosa, it is believed that IAV infection does not progress as rapidly as in mice. Therefore, the progression of IAV infection could be restricted even if IFNλ-PSNPs are delivered 1−2 days after the beginning of IAV replications. We are confident that an inhalation delivery of IFNλ-PSNP, rather than an oral pill or intramuscular injection, can further reduce the activation time of the antiviral mechanism and become a more effective agent for the control of viral infections.

The current data showed that PSNPs enabled more efficient delivery of IFN-λs to the targeted alveolar region and activated potent antiviral immune responses after the onset of IAV infection. Our work has provided further insight into rapid antiviral strategies involving inhaled delivery of IFNλ-PSNPs in an *in vivo* lung to treat IAV-caused lung infection.

https://doi.org/10.1021/acsami.3c13677
ACS Appl. Mater. Interfaces 2024, 16, 11147−11158

EXPERIMENTAL SECTION

Viruses and Reagents. The influenza A virus (A/Wilson-Smith/1933 (A/WS/33) H1N1, ATCC, Manassas, VA, USA) was employed to induce acute respiratory infection in this study. Virus stocks were cultivated in Madin−Darby canine kidney cells using virus growth medium following a standardized protocol.[42] After a 48 h incubation at 37 °C, the supernatants were collected and centrifuged at 5000 rpm for 30 min to eliminate cellular debris. Virus stocks were then assessed for titration on MDCK cells through a TCID assay and stored at −80 °C.

Mice and Virus Inoculation. 7-week-old C57BL/6J (B6) male mice, weighing between 19 and 23 g, obtained from Orientalbio (Seoul, Korea) were employed as wild-type (WT) mice. These B6 mice, like other commercially available inbred mouse strains, carry a nonfunctional Mx1 gene, which originates from mice that are resistant to influenza. All experimental procedures were approved by the Institutional Review Board of the Seoul National University College of Medicine (IRB number 1709-049-883), and the research protocols adhered to the approved guidelines. For viral infections, WT mice were intranasally inoculated with IAV (3.6 × 103 pfu in 30 μL of PBS). Following euthanasia, bronchoalveolar lavage (BAL) fluid was collected from the lungs using 1000 μL of 0.5 mM ethylenediaminetetraacetic acid (EDTA) in phosphate buffered saline (PBS) after tracheal cannulation. The BAL fluid was utilized for enzyme-linked immunosorbent assay (ELISA) to measure secreted protein levels and plaque assay for viral titers determination. Additionally, mouse lungs were harvested for real-time polymerase chain reaction (PCR), immunohistochemistry, and single-cell RNA sequencing (scRNA-seq).

Real-Time PCR. Lung samples were harvested from mice infected with WS/33 (H1N1) for 3, 7, 10, or 14 days, and TRIzol (Invitrogen) was used to extract total RNA. Following this, cDNA synthesis was performed using 3 μg of RNA, Moloney murine leukemia virus reverse transcriptase, and random hexamer primers obtained from PerkinElmer Life Sciences (Waltham, MA, USA) and Roche Applied Science (Indianapolis, IN, USA). The PCR amplification was carried out using TaqMan Universal PCR Master Mix (PE Biosystems, Foster City, CA, USA) as directed by the manufacturer. Each amplification reaction, a total of 12 μL in volume, contained 2 μL of cDNA from the reverse transcription mixture, a TaqMan hybridization probe (at 200 nM), and oligonucleotide primers (at a final concentration of 800 nM). The IAV level was monitored using a quantitative PCR for the *PA* gene (segment 3) with forward and reverse primers and probe 5′-ggccgactacactctcgatga-3′,5′-tgtcttatggtgaatagcctggttt-3′, and 5′-agcag-ggctaggatc-3′, respectively. Primers targeting mouse Mx1, Ifitm1, Ifit2, Rsad2, Cxcl10, and Isg15 were acquired from Applied Biosystems (Foster City, CA, USA). Real-time PCR analysis was conducted using the PE Biosystems ABI PRISM 7700 sequence detection system. The thermal cycling conditions comprised an initial step at 50 °C for 2 min, followed by denaturation at 95 °C for 10 min, and then 40 cycles of denaturation at 95 °C for 15 s and annealing/extension at 60 °C for 1 min. All PCR assays were quantitative and employed plasmids containing the target gene sequences as standards. Triplicate reactions were performed for each sample, and the resulting real-time PCR data were normalized to the expression level of the housekeeping gene glyceraldehyde phosphate dehydrogenase (GAPDH, 1 × 10^6 copies) to account for variations among samples.

Preparation of PSNPs Loaded with GFP or IFN-λs. A 120 mg portion of bovine PS (Newfactan, Yuhan, South Korea) was dissolved in a 12 mL mixture of chloroform (8 mL) and methanol (4 mL) to prepare a 10 mg/mL stock solution. Protamine sulfate (Sigma-Aldrich, MO, USA) was dissolved in deionized water to prepare a 5 mg/mL stock solution. GFP- or IFNλ-PSNP were prepared based on thin-film hydration method. In brief, 5 mg of PS was dried in the lipid film overnight. The PS film was hydrated with a mixture solution of GFP (50 μg/mL) or IFN-λ_2 and IFN-λ_3 (50 μg/mL, R&D system, Minnesota, USA) and protamine sulfate at different molar ratios to the cargo protein (1:1, 1:5, 1:10, and 1:20) and then extruded through a 400 nm membrane at 45 °C. To remove unencapsulated proteins, the extruded solution was dialyzed overnight using a dialysis membrane (100 kDa MWCO, Spectrum Labs). Hydrodynamic size and ζ potential of cargo proteins and PSNPs were measured using a dynamic light scattering (DLS) instrument (Malvern Instruments). Loading efficiency of GFP and IFN-λs was determined by using fluorescence spectrometer (SpectraMax Gemini, Molecular Devices) and Duoset ELISA (DY1789B, R&D systems), respectively. To examine the colloidal stability, GFP-PSNPs or IFNλ-PSNPs were incubated in distilled water containing 10% FBS at 37 °C and the hydrodynamic size change was monitored for 2 h.

Transmission Electron Microscopy. The physical size and morphology of GFP-PSNPs and IFNλ-PSNPs were observed with a field emission-transmission electron microscope (FE-TEM, JEOL USA Inc., Peabody, MA, USA). In brief, 1 mg/mL of PSNPs was mixed with 10% formalin at 1:1 volume ratio for 15 min and applied on a Formvar-carbon coated grid for 1 h. After washing with deionized water three times, the grid was stained with 2% phosphotungstic acid solution for 2 min and dried for 10 min. The grid was then observed with a FE-TEM (200 kV). Loading of IFN-λs in the PSNP was observed with TEM coupled with immunogold labeling. In brief, IFN-$\lambda_{2/3}$ antibody (R&D system) was labeled with 20 nm gold nanoparticles (GNPs) using an InnovaCoat GOLD kit. 1 mg/mL of PSNPs was mixed with 10% formalin at 1:1 volume ratio for 15 min and applied on a Formvar-carbon coated grid for 1 h. After washing with deionized water three times, the grid was treated with 1% BSA blocking solution for 30 min. After washing with deionized water three times, the grid was treated with 5 μg/mL of GNP-labeled IFN-$\lambda_{2/3}$ antibody for 1 h at room temperature. After washing with deionized water three times, the grid was stained with 2% phosphotungstic acid solution for 2 min and dried for 10 min. The grid was then observed with a FE-TEM (200 kV).

***In Vitro* Cellular Experiments.** A549 human lung adenocarcinoma cells and Raw264.7 murine macrophages were cultured in RPMI and DMEM supplemented with 10% FBS and 1% penicillin/streptomycin under a humidified 5% CO_2 atmosphere at 37 °C, respectively. For cytotoxicity, A549 cells were seeded in in a 96-well plate (5000 cells/well). The cells were treated with GFP-PSNPs at different PS concentrations for 1 h and further incubated for 24 h. The cell viability was then examined by MTT assay. For fluorescence imaging, the cells were seeded in a 6-well plate (20 000 cells/well). The cells were treated with GFP-PSNPs at a PS concentration of 0.2 mg/mL for 24 h. After washing with PBS three times, a confocal fluorescence microscope (Nikon Corp., Tokyo, Japan) was used to image the cells.

Inhaled Delivery of PSNPs in IAV-Infected Mice. To examine the colloidal stability under nebulization, the hydrodynamic sizes of GFP-PSNPs before and after nebulization were measured using a DLS instrument (Malvern Instruments). To study the distribution of GFPs in the lung, BALB/c mice were nebulized with GFPs or GFP-PSNPs at a GFP concentration of 15 μg/mL by using the SCIREQ "InExpose" system (SCIREQ, Montreal, QB, Canada). At 1 h after nebulization, mice were transcardially perfused with PBS under anesthesia, and lungs were harvested for fluorescence imaging. The GFP fluorescence in the lungs was imaged by using an *in vivo* fluorescence imaging system (IVIS spectrum, PerkinElmer, Walsham, MA, USA). To study the time-dependent biodistribution of PSNPs, GFP-PSNPs were labeled with 1,1′-dioctadecyl-3,3,3′,3′-tetramethylindotricarbocyanine iodide (DiR, Thermo Fisher Scientific). In brief, 2 μg of DiR was added to the PS solution (5 mg PS) before drying into the lipid film and the following procedure for GFP-PSNP preparation was the same as the above-mentioned procedure. BALB/c mice were nebulized with DiR-labeled GFP-PSNPs at a PS concentration of 1 mg/mL. Mice were transcardially perfused with PBS under anesthesia immediately, at 1, 6, and 24 h after nebulization and major organs including liver, lung, spleen, heart, and kidney were harvested for fluorescence imaging. The DiR and GFP fluorescence in the major organs was imaged by using NIR fluorescence imaging system (Li-COR Biosciences) and IVIS spectrum, respectively. To study the biodistribution of PSNPs at different PS concentrations, BALB/c mice were nebulized with DiR-labeled GFP-PSNPs at PS

https://doi.org/10.1021/acsami.3c13677
ACS Appl. Mater. Interfaces 2024, 16, 11147−11158

concentrations of 1 mg/mL, 2 mg/mL, and 4 mg/mL. To study the cellular distribution of IFN-λs in the lung tissue, BALB/c mice were nebulized with IFN-λs or IFNλ-PSNPs at an IFN-λs concentration of 1 μg/mL. Mice were transcardially perfused with PBS under anesthesia on 1 day and 3 days after nebulization. Lungs were harvested and embedded in optical cutting temperature (OCT) compound. Lung tissue slices were prepared and fixed in 10% (v/v) neutral buffered formalin for 10 min. After washing with PBS three times, the lung tissue slices were treated with 0.2% Triton X-100 (Sigma-Aldrich) for 10 min. After washing with PBS three times, the lung tissue slices were treated with 5% BSA blocking solution for 30 min. After washing with PBS three times, the lung tissue slices were treated with 5 μg/mL of IFN-λ 2/3 primary antibody (R&D systems) overnight at 4 °C. After washing with PBS three times, the lung tissue slices were treated with 2 μg/mL of Alexa Fluor 647-labeled secondary antibody (A-21247, Thermo Fisher scientific) for 30 min at room temperature. After being washed with PBS three times, the lung tissue slices were imaged using a confocal fluorescence microscope (Nikon, Japan). To study antiviral effects of inhaled IFN-λs and IFNλ-PSNPs, B6 mice were infected with IAV (3.6×10^3 pfu/30 μL, WS/H1N1) and immediately nebulized with IFN-λs or IFNλ-PSNPs at an IFN-λs concentration of 1 μg/mL. Lungs were harvested immediately and 3, 7, 10, and 14 days after inhalation.

Immunohistochemistry and Histological Analysis. Lung tissues were fixed in 10% (v/v) neutral buffered formalin and embedded in paraffin. The paraffin-embedded tissue sections were stained with hematoxylin and eosin (H&E) solution from Sigma-Aldrich (St. Louis, MO, USA). Evaluation of inflammatory cells in H&E-stained lung sections was performed using a semiquantitative scoring system in a blinded manner, as previously outlined. Histopathological analysis included the examination of lung sections from a minimum of three B6 mice, with scores ranging from zero to three points based on the degree of inflammatory cell infiltration into lung tissue: 0 for normal, 1 for a single-layer ring of inflammatory cells, 2 for a ring of inflammatory cells two to four cells deep, and 3 for a ring of inflammatory cells exceeding four cells deep. The histological score for control hamster lung tissue treated with PBS/PBS consistently registered zero points. Evaluation entailed the examination of at least five different regions within similar sections from each hamster, with a minimum of three hamsters analyzed per condition. Inflammatory cell infiltration was quantified by a blinded examiner and expressed as the number of cells per high-power field.

Western Blot Analysis. The expression of the IAV NP protein was evaluated through Western blot analysis. Lung tissue from mice was lysed using 2× lysis buffer containing 250 mM Tris-Cl (pH 6.5), 2% SDS, 4% β-mercaptoethanol, 0.02% bromophenol blue, and 10% glycerol. A total of 30 μg of protein from the cell lysate was electrophoresed in 10% SDS gels and subsequently transferred to polyvinylidene difluoride membranes in Tris-buffered saline (TBS; 50 mM Tris-Cl, pH 7.5, 150 mM NaCl) at room temperature for 1 h. Subsequently, the membrane was left to incubate overnight with a primary antibody (dilution 1:500) in Tween-Tris buffered saline (TTBS; 0.5% Tween-20 in TBS). After rinsing with TTBS, the blot underwent a 1 h incubation at room temperature with a secondary antirabbit or antimouse antibody (dilution 1:1000, sourced from Cell Signaling, Beverly, MA, USA) in TTBS. Visualization was achieved using an ECL system (Amersham, Little Chalfont, U.K.).

Statistical Analyses. A graphical representation of a representative experiment, consisting of five mice per group, was generated from three repeated experiments. The *in vivo* results of real-time PCR are presented as mean ± SD values obtained from five individual mice, and differences between treatment groups were assessed using repeated measure two-way analysis of variance (ANOVA). Single-cell RNA sequencing data were analyzed using two-sample *t* tests. Statistical analyses were conducted using GraphPad Prism (version 8; GraphPad Software, La Jolla, CA, USA), with significance determined at $p < 0.05$.

■ ASSOCIATED CONTENT

Data Availability Statement

All data needed to evaluate the conclusions in the paper are present in the paper and/or the Supporting Information.

Supporting Information

The Supporting Information is available free of charge at https://pubs.acs.org/doi/10.1021/acsami.3c13677.

Optimization of GFP-loaded pulmonary surfactant nanoparticles (GFP-PSNPs) by varying the molar ratio of protamine to GFP (Figure S1); intracellular delivery of GFPs via GFP-protamine complexes and GFP-PSNPs (Figure S2); time-dependent biodistribution of GFPs after inhalation of free GFPs (Figure S3); kinetics of IAV infection *in vivo* (Figure S4); IFNλ-PSNPs inducing more effective antiviral immune responses in the lung of IAV-infected mice (Figure S5); inhaled delivery of IFNβ-PSNPs in the lungs of mice infected with IAV (Figure S6); single-cell RNA sequencing analysis of the whole lung tissues of C57BL/6 mice infected with influenza A virus (Figure S7); molecular weight and ζ potential of interferon-λ and GFP (Table S1); colloidal stability of GFP-PSNPs (Table S2) (PDF)

■ AUTHOR INFORMATION

Corresponding Authors

Su-Hyung Park − *Graduate School of Medical Science & Engineering, Korea Advanced Institute of Science and Technology, Daejeon 34141, Korea; The Center for Epidemic Preparedness, KAIST Institute, Daejeon 34141, Korea*; Phone: +82-42-350-4248; Email: park3@kaist.ac.kr; Fax: +82-42-350-4240

Ji-Ho Park − *Department of Bio and Brain Engineering and KAIST Institute for Health Science and Technology, Korea Advanced Institute of Science and Technology, Daejeon 34141, Korea*; orcid.org/0000-0002-0721-0428; Phone: +82-42-350-4330; Email: jihopark@kaist.ac.kr; Fax: +82-42-350-4310

Hyun Jik Kim − *Department of Otorhinolaryngology, Seoul National University College of Medicine, Seoul 03080, Korea; Seoul National University Hospital, Seoul 03080, Korea; Sensory Organ Research Institute, Seoul National University Medical Research Center, Seoul 03080, Korea*; orcid.org/0000-0001-8631-928X; Phone: +82-2-2228-2203; Email: hyunjerry@snu.ac.kr; Fax: +82-2-745-2387

Authors

Chan Hee Gil − *Department of Otorhinolaryngology, Seoul National University College of Medicine, Seoul 03080, Korea*

Chanhee Oh − *Department of Bio and Brain Engineering and KAIST Institute for Health Science and Technology, Korea Advanced Institute of Science and Technology, Daejeon 34141, Korea*; orcid.org/0000-0002-5913-0075

Jeongsoo Lee − *Graduate School of Medical Science & Engineering, Korea Advanced Institute of Science and Technology, Daejeon 34141, Korea*

Mincheol Jang − *Department of Bio and Brain Engineering and KAIST Institute for Health Science and Technology, Korea Advanced Institute of Science and Technology, Daejeon 34141, Korea*

Junhee Han − *Department of Bio and Brain Engineering and KAIST Institute for Health Science and Technology, Korea*

https://doi.org/10.1021/acsami.3c13677
ACS Appl. Mater. Interfaces 2024, 16, 11147−11158

Advanced Institute of Science and Technology, Daejeon 34141, Korea

Sung-Dong Cho − *Graduate School of Medical Science & Engineering, Korea Advanced Institute of Science and Technology, Daejeon 34141, Korea*

Complete contact information is available at: https://pubs.acs.org/10.1021/acsami.3c13677

Author Contributions

[¶]C.H.G., C.O., J.L., and M.J. contributed equally to this work.

Notes

Ethics Statement. *In vivo* experiments with C57BL/6 mice were carried out according to guidelines approved by the Institutional Review Boards of the Seoul National University College of Medicine and the Korea Advanced Institute of Science and Technology (IACUC Nos. 2016-0093 and KA2020-46).

The authors declare no competing financial interest.

■ ACKNOWLEDGMENTS

This work was supported by the Basic Science Research Program through the National Research Foundation of Korea, funded by the Ministry of Education (2022R1A2C2011867) awarded to H.J.K. and by the Ministry of Science and ICT (RS-2023-00222762) awarded to H.J.K. This research was also supported by a grant from the Korean Health Technology R&D Project through the Korean Health Industry Development Institute, funded by the Ministry of Health & Welfare of the Republic of Korea (HI23C0795 awarded to H.J.K.).

■ REFERENCES

(1) Lowery, S. A.; Sariol, A.; Perlman, S. Innate immune and inflammatory responses to SARS-CoV-2: Implications for COVID-19. *Cell Host Microbe* **2021**, *29*, 1052−1062.

(2) Blanco-Melo, D.; Nilsson-Payant, B. E.; Liu, W. C.; Uhl, S.; Hoagland, D.; Møller, R.; Jordan, T. X.; Oishi, K.; Panis, M.; Sachs, D.; Wang, T. T.; Schwartz, R. E.; Lim, J. K.; Albrecht, R. A.; tenOever, B. R. Imbalanced Host Response to SARS-CoV-2 Drives Development of COVID-19. *Cell* **2020**, *181*, 1036−1045.

(3) Kim, H. J.; Jo, A.; Jeon, Y. J.; An, S.; Lee, K. M.; Yoon, S. S.; Choi, J. Y. Nasal commensal Staphylococcus epidermidis enhances interferon-λ-dependent immunity against influenza virus. *Microbiome* **2019**, *7*, 80.

(4) Kim, S.; Kim, M. J.; Kim, C. H.; Kang, J. W.; Shin, H. K.; Kim, D. Y.; Won, T. B.; Han, D. H.; Rhee, C.-S.; Yoon, J. H.; Kim, H. J. The Superiority of IFN-λ as a Therapeutic Candidate to Control Acute Influenza Viral Lung Infection. *Am. J. Respir. Cell Mol. Biol.* **2017**, *56*, 202−212.

(5) Major, J.; Crotta, S.; Llorian, M.; McCabe, T. M.; Gad, H. H.; Priestnall, S. L.; Hartmann, R.; Wack, A. Type I and III interferons disrupt lung epithelial repair during recovery from viral infection. *Science* **2020**, *369*, 712−717.

(6) Hemann, E. A.; Green, R.; Turnbull, J. B.; Langlois, R. A.; Savan, R.; Gale, M., Jr Interferon-λ modulates dendritic cells to facilitate T cell immunity during infection with influenza A virus. *Nat. Immunol* **2019**, *20*, 1035−1045.

(7) An, S.; Jeon, Y. J.; Jo, A.; Lim, H. J.; Han, Y. E.; Cho, S. W.; Kim, H. Y.; Kim, H. J. Initial Influenza Virus Replication Can Be Limited in Allergic Asthma Through Rapid Induction of Type III Interferons in Respiratory Epithelium. *Front. Immunol.* **2018**, *9*, 986.

(8) Galani, I. E.; Triantafyllia, V.; Eleminiadou, E. E.; Koltsida, O.; Stavropoulos, A.; Manioudaki, M.; Thanos, D.; Doyle, S. E.; Kotenko, S. V.; Thanopoulou, K.; Andreakos, E. Interferon-λ Mediates Non-redundant Front-Line Antiviral Protection against Influenza Virus Infection without Compromising Host Fitness. *Immunity* **2017**, *46*, 875−890.

(9) Davidson, S.; McCabe, T. M.; Crotta, S.; Gad, H. H.; Hessel, E. M.; Beinke, S.; Hartmann, R.; Wack, A. IFNλ is a potent anti-influenza therapeutic without the inflammatory side effects of IFNα treatment. *EMBO Mol. Med.* **2016**, *8*, 1099−1112.

(10) Chong, Z.; Karl, C. E.; Halfmann, P. J.; Kawaoka, Y.; Winkler, E. S.; Keeler, S. P.; Holtzman, M. J.; Yu, J.; Diamond, M. S. Nasally delivered interferon-λ protects mice against infection by SARS-CoV-2 variants including Omicron. *Cell Rep* **2022**, *39*, No. 110799.

(11) Jeon, Y. H.; Gil, C. H.; Jo, A.; Won, J.; Kim, S.; Kim, H. J. The influence of interferon-lambda on restricting Middle East Respiratory Syndrome Coronavirus replication in the respiratory epithelium. *Antiviral Res.* **2020**, *180*, No. 104860.

(12) Liu, Q.; Xue, J.; Zhang, X.; Chai, J.; Qin, L.; Guan, J.; Zhang, X.; Mao, S. The influence of a biomimetic pulmonary surfactant modification on the in vivo fate of nanoparticles in the lung. *Acta Biomater* **2022**, *147*, 391−402.

(13) Sanches Santos Rizzo Zuttion, M.; Moore, S. K. L.; Chen, P.; Beppu, A. K.; Hook, J. L. New Insights into the Alveolar Epithelium as a Driver of Acute Respiratory Distress Syndrome. *Biomolecules* **2022**, *12*, 1273.

(14) Yue, P.; Zhou, W.; Huang, G.; Lei, F.; Chen, Y.; Ma, Z.; Chen, L.; Yang, M. Nanocrystals based pulmonary inhalation delivery system: advance and challenge. *Drug Deliv* **2022**, *29*, 637−651.

(15) Ruge, C. A.; Schaefer, U. F.; Herrmann, J.; Kirch, J.; Cañadas, O.; Echaide, M.; Pérez-Gil, J.; Casals, C.; Müller, R.; Lehr, C. M. The interplay of lung surfactant proteins and lipids assimilates the macrophage clearance of nanoparticles. *PLoS One* **2012**, *7*, No. e40775.

(16) Guagliardo, R.; Pérez-Gil, J.; De Smedt, S.; Raemdonck, K. Pulmonary surfactant and drug delivery: Focusing on the role of surfactant proteins. *Control Release* **2018**, *291*, 116−126.

(17) Carregal-Romero, S.; Groult, H.; Cañadas, O.; A-Gonzalez, N.; Lechuga-Vieco, A. V.; García-Fojeda, B.; Herranz, F.; Pellico, J.; Hidalgo, A.; Casals, C.; Ruiz-Cabello, J. Delayed alveolar clearance of nanoparticles through control of coating composition and interaction with lung surfactant protein A. *Biomater Adv.* **2022**, *134*, No. 112551.

(18) Shin, H.; Kim, S.; Jo, A.; Won, J.; Gil, C. H.; Yoon, S. Y.; Cha, H.; Kim, H. J. Intranasal inoculation of IFN-λ resolves SARS-CoV-2 lung infection via the rapid reduction of viral burden and improvement of tissue damage. *Front. Immunol.* **2022**, *13*, No. 1009424.

(19) Watson, A.; Spalluto, C. M.; McCrae, C.; Cellura, D.; Burke, H.; Cunoosamy, D.; Freeman, A.; Hicks, A.; Hühn, M.; Ostridge, K.; Staples, K. J.; Vaarala, O.; Wilkinson, T. Dynamics of IFN-β Responses during Respiratory Viral Infection. Insights for Therapeutic Strategies. *Am. J. Respir Crit Care Med.* **2020**, *201*, 83−94.

(20) Korsunsky, I.; Millard, N.; Fan, J.; Slowikowski, K.; Zhang, F.; Wei, K.; Baglaenko, Y.; Brenner, M.; Loh, P. R.; Raychaudhuri, S. Fast, sensitive and accurate integration of single-cell data with Harmony. *Nat. Methods* **2019**, *16*, 1289−1296.

(21) Lee, J. S.; Koh, J. Y.; Yi, K.; Kim, Y. I.; Park, S. J.; Kim, E. H.; Kim, S. M.; Park, S. H.; Ju, Y. S.; Choi, Y. K.; Park, S. H. Single-cell transcriptome of bronchoalveolar lavage fluid reveals sequential change of macrophages during SARS-CoV-2 infection in ferrets. *Nat. Commun.* **2021**, *12*, 4567.

(22) Benam, K. H.; Denney, L.; Ho, L. P. How the Respiratory Epithelium Senses and Reacts to Influenza Virus. *Am. J. Respir. Cell Mol. Biol.* **2019**, *60*, 259−268.

(23) Xi, B.; Zeng, X.; Chen, Z.; Zeng, J.; Huang, L.; Du, H. SARS-CoV-2 within-host diversity of human hosts and its implications for viral immune evasion. *mBio* **2023**, *5*, No. e0067923.

(24) Dittmann, M.; Hoffmann, H. H.; Scull, M. A.; Gilmore, R. H.; Bell, K. L.; Ciancanelli, M.; Wilson, S. J.; Crotta, S.; Yu, Y.; Flatley, B.; Xiao, J. W.; Casanova, J. L.; Wack, A.; Bieniasz, P. D.; Rice, C. M. A serpin shapes the extracellular environment to prevent influenza A virus maturation. *Cell* **2015**, *160*, 631−643.

(25) Iwasaki, A.; Pillai, P. S. Innate immunity to influenza virus infection. *Nat. Rev. Immunol* **2014**, *14*, 315−328.
(26) Pang, I. K.; Iwasaki, A. Inflammasomes as mediators of immunity against influenza virus. *Trends Immunol* **2011**, *32*, 34−41.
(27) Brandi, P.; Conejero, L.; Cueto, F. J.; Martínez-Cano, S.; Dunphy, G.; Gómez, M. J.; Relaño, C.; Saz-Leal, P.; Enamorado, M.; Quintas, A.; Dopazo, A.; Amores-Iniesta, J.; Del Fresno, C.; Nistal-Villán, E.; Ardavin, C.; Nieto, A.; Casanovas, M.; Subiza, J. L.; Sancho, D. Trained immunity induction by the inactivated mucosal vaccine MV130 protects against experimental viral respiratory infections. *Cell Rep* **2022**, *38*, No. 110184.
(28) Mettelman, R. C.; Allen, E. K.; Thomas, P. G. Mucosal immune responses to infection and vaccination in the respiratory tract. *Immunity* **2022**, *55*, 749−780.
(29) Acharya, D.; Reis, R.; Volcic, M.; Liu, G.; Wang, M. K.; Chia, B. S.; Nchioua, R.; Groß, R.; Münch, J.; Kirchhoff, F.; Sparrer, K. M. J.; Gack, M. U. Actin cytoskeleton remodeling primes RIG-I-like receptor activation. *Cell* **2022**, *185*, 3588−3602.
(30) French, H.; Pitré, E.; Oade, M. S.; Elshina, E.; Bisht, K.; King, A.; Bauer, D. L. V.; Te Velthuis, A. J. W. Transient RNA structures cause aberrant influenza virus replication and innate immune activation. *Sci. Adv.* **2022**, *8*, No. eabp8655.
(31) Zhou, Z.; Ren, L.; Zhang, L.; Zhong, J.; Xiao, Y.; Jia, Z.; Guo, L.; Yang, J.; Wang, C.; Jiang, S.; Yang, D.; Zhang, G.; Li, H.; Chen, F.; Xu, Y.; Chen, M.; Gao, Z.; Yang, J.; Dong, J.; Liu, B.; Zhang, X.; Wang, W.; He, K.; Jin, Q.; Li, M.; Wang, J. Heightened Innate Immune Responses in the Respiratory Tract of COVID-19 Patients. *Cell Host Microbe* **2020**, *27*, 883−890.
(32) Won, J.; Jo, A.; Gil, C. H.; Kim, S.; Shin, H.; Kim, H. J. Inhaled delivery of recombinant interferon-lambda restores allergic inflammation after development of asthma by controlling Th2- and Th17-cell-mediated immune responses. *Int. Immunopharmacol.* **2022**, *112*, No. 109180.
(33) Watson, A.; Spalluto, C. M.; McCrae, C.; Cellura, D.; Burke, H.; Cunoosamy, D.; Freeman, A.; Hicks, A.; Hühn, M.; Ostridge, K.; Staples, K. J.; Vaarala, O.; Wilkinson, T. Dynamics of IFN-β Responses during Respiratory Viral Infection. Insights for Therapeutic Strategies. *Am. J. Respir Crit Care Med.* **2020**, *201*, 83−94.
(34) Hoagland, D. A.; Møller, R.; Uhl, S. A.; Oishi, K.; Frere, J.; Golynker, I.; Horiuchi, S.; Panis, M.; Blanco-Melo, D.; Sachs, D.; Arkun, K.; Lim, J. K.; tenOever, B. R. Leveraging the antiviral type I interferon system as a first line of defense against SARS-CoV-2 pathogenicity. *Immunity* **2021**, *54*, 557−570.
(35) Park, A.; Iwasaki, A. Type I and Type III Interferons - Induction, Signaling, Evasion, and Application to Combat COVID-19. *Cell Host Microbe* **2020**, *27*, 870−878.
(36) Karlowitz, R.; Stanifer, M. L.; Roedig, J.; Andrieux, G.; Bojkova, D.; Bechtel, M.; Smith, S.; Kowald, L.; Schubert, R.; Boerries, M.; Cinatl, J., Jr.; Boulant, S.; van Wijk, S. J. L. USP22 controls type III interferon signaling and SARS-CoV-2 infection through activation of STING. *Cell Death Dis.* **2022**, *13*, 684.
(37) Rich, H. E.; Antos, D.; Melton, N. R.; Alcorn, J. F.; Manni, M. L. Insights into Type I and III Interferons in Asthma and Exacerbations. *Front Immunol* **2020**, *11*, No. 574027.
(38) Lamers, M. M.; van der Vaart, J.; Knoops, K.; Riesebosch, S.; Breugem, T. I.; Mykytyn, A. Z.; Beumer, J.; Schipper, D.; Bezstarosti, K.; Koopman, C. D.; Groen, N.; Ravelli, R. B. G.; Duimel, H. Q.; Demmers, J. A. A.; Verjans, G. M. G. M.; Koopmans, M. P. G.; Muraro, M. J.; Peters, P. J.; Clevers, H.; Haagmans, B. L. An organoid-derived bronchioalveolar model for SARS-CoV-2 infection of human alveolar type II-like cells. *EMBO J.* **2021**, *40*, No. e105912.
(39) Stegemann-Koniszewski, S.; Jeron, A.; Gereke, M.; Geffers, R.; Kröger, A.; Gunzer, M.; Bruder, D. Alveolar Type II Epithelial Cells Contribute to the Anti-Influenza A Virus Response in the Lung by Integrating Pathogen- and Microenvironment-Derived Signals. *mBio* **2016**, *7*, No. e00276-16.
(40) Hidalgo, A.; Cruz, A.; Pérez-Gil, J. Barrier or carrier? Pulmonary surfactant and drug delivery. *Eur. J. Pharm. Biopharm* **2015**, *95*, 117−127.
(41) Wang, J.; Li, P.; Yu, Y.; Fu, Y.; Jiang, H.; Lu, M.; Sun, Z.; Jiang, S.; Lu, L.; Wu, M. X. Pulmonary surfactant-biomimetic nanoparticles potentiate heterosubtypic influenza immunity. *Science* **2020**, *367*, eaau0810.
(42) Jo, A.; Won, J.; Gil, C. H.; Kim, S. K.; Lee, K. M.; Yoon, S. S.; Kim, H. J. Nasal symbiont Staphylococcus epidermidis restricts the cellular entry of influenza virus into the nasal epithelium. *npj Biofilms Microbiomes* **2022**, *8*, 26.

https://doi.org/10.1021/acsami.3c13677
ACS Appl. Mater. Interfaces 2024, 16, 11147−11158